# Local structure of stoichiometric and oxygen-deficient $A_2Ti_6O_{13}$ (A = Li, Na, and K) studied by X-ray absorption spectroscopy and first-principles calculations

Jarin Kanchanawarin, Wanwisa Limphirat, Pratya Promchana, Tawan Sooknoi, Tosapol Maluangnont, Kodchakorn Simalaotao, Adisak Boonchun, Pakpoom Reunchan, Sukit Limpijumnong, and Jiraroj T-Thienprasert

Citation: Journal of Applied Physics **124**, 155101 (2018); doi: 10.1063/1.5052032
View online: https://doi.org/10.1063/1.5052032
View Table of Contents: http://aip.scitation.org/toc/jap/124/15
Published by the American Institute of Physics

# Local structure of stoichiometric and oxygen-deficient $A_2Ti_6O_{13}$ ($A$ = Li, Na, and K) studied by X-ray absorption spectroscopy and first-principles calculations

Jarin Kanchanawarin,[1] Wanwisa Limphirat,[2] Pratya Promchana,[3,4] Tawan Sooknoi,[3,4] Tosapol Maluangnont,[3,5,a)] Kodchakorn Simalaotao,[1] Adisak Boonchun,[1,6] Pakpoom Reunchan,[1,6] Sukit Limpijumnong,[6,7,b)] and Jiraroj T-Thienprasert[1,6,a)]

[1]*Department of Physics, Faculty of Science, Kasetsart University, Bangkok 10900, Thailand*
[2]*Synchrotron Light Research Institute (Public Organization), Nakhon Ratchasima 30000, Thailand*
[3]*Catalytic Chemistry Research Unit, Faculty of Science, King Mongkut's Institute of Technology Ladkrabang, Bangkok 10520, Thailand*
[4]*Department of Chemistry, Faculty of Science, King Mongkut's Institute of Technology Ladkrabang, Bangkok 10520, Thailand*
[5]*College of Nanotechnology, King Mongkut's Institute of Technology Ladkrabang, Bangkok 10520, Thailand*
[6]*Thailand Center of Excellence in Physics (ThEP Center), Commission on Higher Education, Bangkok 10400, Thailand*
[7]*School of Physics and NANOTEC-SUT Center of Excellence on Advance Functional Nanomaterials, Suranaree University of Technology, Nakhon Ratchasima 30000, Thailand*

(Received 14 August 2018; accepted 19 September 2018; published online 15 October 2018)

Oxygen vacancy defects ($V_O$) in Ti-based oxides play important roles in catalytic processes despite limited knowledge regarding their formation and characterization. Here, we demonstrate the use of X-ray absorption spectroscopy (XAS) measurements to compare the *relative* proportion of $V_O$ defects in as-grown alkali hexatitanate $A_2Ti_6O_{13}$ ($A$ = Li, Na, K). Both X-ray absorption near edge structure (XANES) and extended X-ray absorption fine structure (EXAFS) regions were studied. The similarity of measured XANES spectra of Ti $K$-edge in all samples indicates the presence of $(Ti^{4+})O_6$ units in good agreement with reported X-ray diffraction results. The small influence of cations $A$ at the tunnel was observed and can be well reproduced in the simulated spectra. In addition, we present a semi-quantitative approach to intuitively determine the content of $V_O$ defects in oxygen-deficient $K_2Ti_6O_{13-x}$ by *in situ* time-resolved XAS measurements under reducing conditions (10%$H_2$/Ar, 50-650 °C). The *in situ* XANES measurements indicate that the oxidation state of bulk Ti remains the same as the as-grown sample, i.e., 4+, at elevated temperatures. By *in situ* EXAFS measurements, the relative number of $V_O$ defects is highest at a reduction temperature of ~550 °C and slightly decreases after that. To confirm the formation of $V_O$ defects, first-principles calculations were independently carried out using a 126-atom $K_2Ti_6O_{13}$ supercell with $V_O$ at various positions. Based on calculated EXAFS, the removal of the oxygen atom nearest to the tunnel, which is the lowest energy structure, provides a good match to the experimental spectra. *Published by AIP Publishing.* https://doi.org/10.1063/1.5052032

## I. INTRODUCTION

The utilization of Ti-based oxides in several applications relies on the reactivity of negatively-charged oxygen atoms in response to the interacting species.[1–4] For example, the exposure of $TiO_2$ to $NH_3$ induced the partial substitution of N for O,[5,6] extending its photocatalytic activity to the visible-light region. In another scenario, the oxygen vacancy defects $V_O$ could be generated via $H_2$-treatment, acting as the catalytically active site in the ketonization of carboxylic acid.[7] The formation of $V_O$ defects can be indirectly detected by electron paramagnetic resonance (EPR)[8,9] or thermal-desorption spectroscopy (TDS) measurements.[9,10] Meanwhile, the long-range structure including the position and content of $V_O$ defects can be determined from neutron diffraction.[11] However, because several types of crystallographically inequivalent oxygen atoms might exist, it is not clear which atoms possess the highest reactivity, leading to $V_O$ defects. The understanding of the "structure" at different length scales from local to long-range is therefore of paramount importance for materials engineering and properties design.

Among several types of technologically important oxides, those based on the Andersson-Wadsley[12–16] family ($A_2O{\cdot}nTiO_2$; $A$ = alkali cation; $1 \le n \le 6$) have received increasing attention. The $n = 6$ members, i.e., alkali hexatitanate $A_2Ti_6O_{13}$, have been extensively studied for several potential applications.[17–27] The crystal structure of $K_2Ti_6O_{13}$ (space group $C2/m$)[28,29] is shown in Fig. 1. Three $TiO_6$ octahedra are edge-shared in a row forming a building block, and the block connected with identical blocks at above as well as below resulting in a ribbon. The ribbons are corner-shared, resulting in a $(Ti_6O_{13})^{2-}$ framework with the tunnel extending

a)Authors to whom correspondence should be addressed: tosapol.ma@kmitl.ac.th and fscicwt@ku.ac.th
b)Present address: The Institute for the Promotion of Teaching Science and Technology, 924 Sukhumvit Road, Phra Khanong, Klong Toei, Bangkok 10110, Thailand.

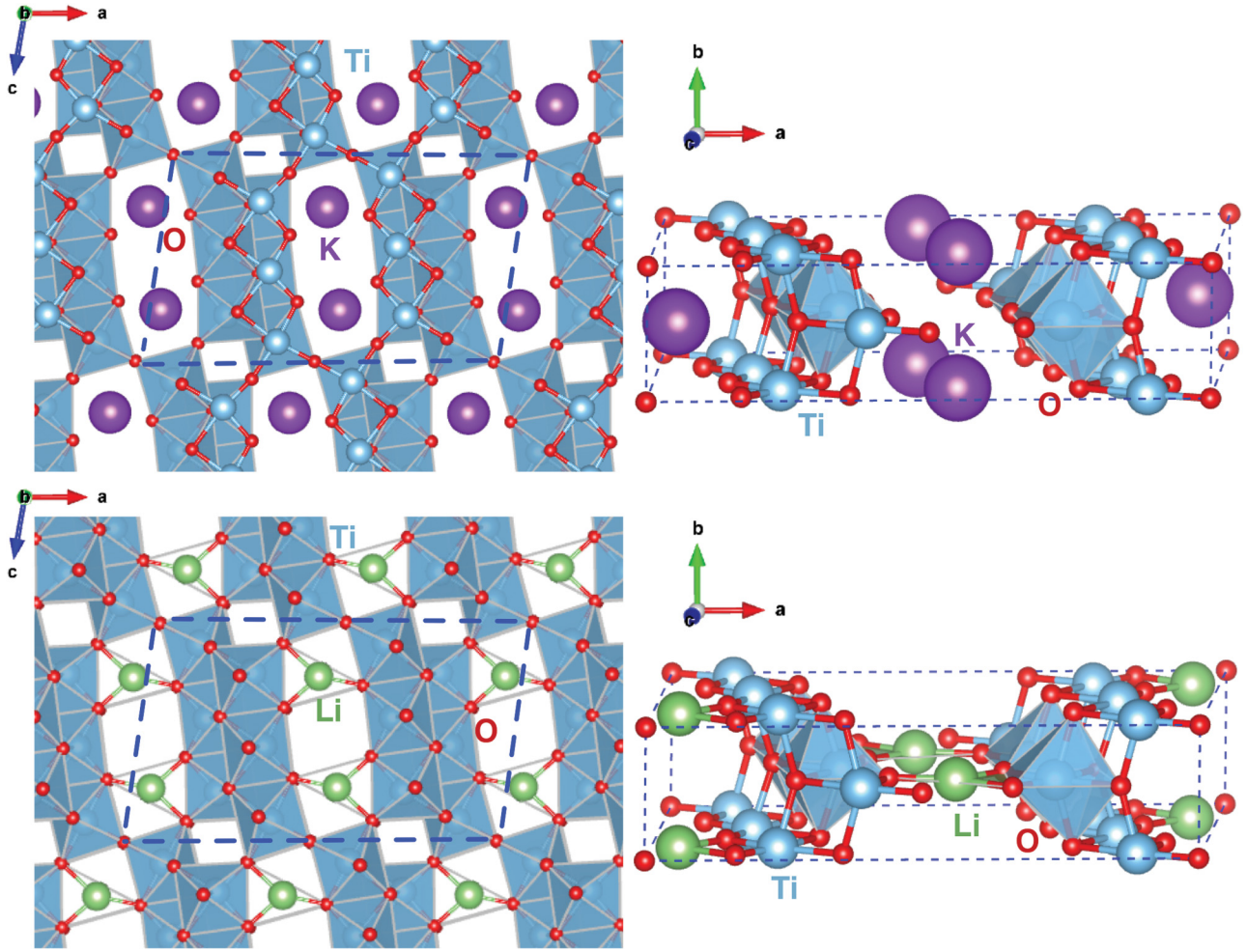


FIG. 1. Illustrations of (top) $K_2Ti_6O_{13}$ and (bottom) $Li_2Ti_6O_{13}$ crystal structures. The dashed blue line represents the 42-atom unit cell. The purple, green, red, and blue spheres represent K, Li, O, and Ti atoms, respectively. Note that the crystal structure of $Na_2Ti_6O_{13}$ (not shown) is similar to that of $K_2Ti_6O_{13}$.

along the *b*-direction. Based on symmetries, there are seven types of the oxygen atoms in this structure with a coordination number ranging from 2 to 4. The larger $K^+$ (and $Na^+$) cations coordinate to eight oxygen atoms in a distorted tetragonal prism $(K/Na)O_8$. On the contrary, the smaller $Li^+$ cations form a distorted $LiO_3$ triangular geometry.[21,22,24,29,30] While the long-range structure of $A_2Ti_6O_{13}$ ($A$ = Li, Na, K) is adequately understood, the influence of $A$ on its local structure has not been studied to the best of our knowledge.

The local structures of Ti in a variety of Ti-bearing crystalline oxides have been successfully investigated by X-ray absorption spectroscopy (XAS) technique, including both X-ray absorption near-edge structure (XANES) and extended X-ray absorption fine structure (EXAFS).[31] In this article, we first study the local structures around Ti atoms in stoichiometric, as-grown $A_2Ti_6O_{13}$ ($A$ = Li, Na, and K) and compare them to the reported crystal structures.[21,22,24,29,30] Here, XAS measurements have allowed us to compare the relative proportion of $V_O$ defects in the as-grown samples. Next, we report the *in situ* time-resolved Ti *K*-edge XANES and the corresponding EXAFS spectra of the oxygen-deficient $K_2Ti_6O_{13-x}$ under exposure to gaseous $H_2$ at 50-650 °C. When $K_2Ti_6O_{13}$ is exposed to $H_2$, the following reaction is expected:

$$K_2(Ti^{4+})_6O_{13} + xH_2 \rightarrow K_2(Ti^{4+})_{6-2x}(Ti^{3+})_{2x}O_{13-x}(V_O)_x + xH_2O. \quad (1)$$

A combination of synchrotron XAS measurements and first-principles calculations is a powerful means for the structural identification of impurities in materials with a high degree of confidence.[4,32–37] So, we will also report the optimized structure obtained *via* first-principles calculations, where the different reactivity of oxygen atoms at multiple crystallographic positions are elucidated and compared to previous reports.[38–40] Our work provides an improved understanding of the local structure around $V_O$ defects under the conditions where they are generated, complementing the information regarding the long-range structure typically obtained via X-ray diffraction (XRD) and other *ex situ* characterizations. In addition, we demonstrate herein the application of *in situ* EXAFS measurements as an intuitive way to estimate the *relative* proportion of reduced Ti atoms at elevated temperatures.

TABLE I. Lattice parameters of $A_2Ti_6O_{13}$ ($A$ = Li, Na, K).

| Materials | Lattice parameters | | |
|---|---|---|---|
| | Calculation | XRD[a] | XRD[b] |
| $Li_2Ti_6O_{13}$ | $a$ = 15.538 Å | $a$ = 15.32(7) Å | $a$ = 15.3065 Å |
| | $b$ = 3.778 Å | $b$ = 3.79(1) Å | $b$ = 3.74739 Å |
| | $c$ = 9.251 Å | $c$ = 9.10(3) Å | $c$ = 9.1404 Å |
| | $\beta$ = 99.636° | $\beta$ = 99.9(3)° | $\beta$ = 99.379° |
| $Na_2Ti_6O_{13}$ | $a$ = 15.274 Å | $a$ = 15.084(8) Å | $a$ = 15.11 Å |
| | $b$ = 3.763 Å | $b$ = 3.744(1) Å | $b$ = 3.744 Å |
| | $c$ = 9.281 Å | $c$ = 9.166(5) Å | $c$ = 9.1693 Å |
| | $\beta$ = 98.949° | $\beta$ = 99.04(3)° | $\beta$ = 98.984° |
| $K_2Ti_6O_{13}$ | $a$ = 15.829 Å | $a$ = 15.59(2) Å | $a$ = 15.582 Å |
| | $b$ = 3.818 Å | $b$ = 3.795(2) Å | $b$ = 3.82 Å |
| | $c$ = 9.246 Å | $c$ = 9.09(1) Å | $c$ = 9.112 Å |
| | $\beta$ = 100.265° | $\beta$ = 99.90(9)° | $\beta$ = 99.764° |

[a]From this work; the standard deviation at the last digit in parentheses.
[b]From other works (Refs. 22 and 29).

## II. EXPERIMENTAL AND CALCULATION METHODS

### A. Solid state synthesis

$K_2Ti_6O_{13}$ was made via a low-temperature solid state synthesis method[41] by calcining the stoichiometric mixture of $KNO_3$ and P25-$TiO_2$ at 700 °C for 10 h. $Na_2Ti_6O_{13}$ was grown by calcining the stoichiometric mixture of $Na_2CO_3$ and anatase $TiO_2$ at 800 °C for 20 h.[42] $Li_2Ti_6O_{13}$ was prepared from $Na_2Ti_6O_{13}$ via the sodium/lithium ion exchange in molten $LiNO_3$ at 380 °C.[24] All prepared samples are in the form of white powder. To evaluate overall crystal structure and quality, XRD measurements were performed using a Rigaku DMAX 2200/Ultima+ diffractometer (Cu K$\alpha$, 40 kV, 30 mA). The XRD patterns and the corresponding unit cell parameters of $A_2Ti_6O_{13}$ synthesized are in good agreement with the reported ones as shown in Table I.[22,29] To analyze specific local structures around Ti atoms, the XAS measurements were performed as described below.

### B. X-ray absorption spectroscopy measurement

The XAS technique was performed to investigate the local structures of as made $A_2Ti_6O_{13}$ ($A$ = Li, Na, K) samples. In this work, the Ti $K$-edge XANES and EXAFS measurements were carried out in the transmission mode using ionization chambers as the detectors at the X-ray absorption beamline (BL-5) of the Siam photon source (electron energy of ~1.2 GeV and beam current of 120–80 mA), Synchrotron Light Research Institute (SLRI), Thailand. A double crystal monochromator with Ge(220) was used to scan the photon energy with the energy step of 0.20 eV in the energy range of 4900 to 5050 eV for XANES region. The scanning was continued with the energy step of 1 eV for the energy range of 5050 to 5600 eV to cover the EXAFS region. After obtaining the raw data, the data processing for XAS analysis, including pre-edge subtraction, post-edge subtraction, background subtraction, and normalization, were performed according to the standard analysis technique described by Ravel and Newville.[43] Regarding EXAFS spectra in $k$-space $\chi(k)$, we choose to plot $k^2\chi(k)$ to enhance the EXAFS signal in the high $k$-region. Fourier transforms as implemented in ATHENA package[43] were then applied to obtain a real-space (R-space) representation of EXAFS spectra $\tilde{\chi}(R)$ according to the following relation:

$$\tilde{\chi}(R) = \frac{1}{\sqrt{2\pi}} \int_0^\infty k^2 \chi(k) W(k) e^{i2kR} dk, \quad (2)$$

where $W(k)$ is the Hanning window.

To gain a deeper understanding of the change in the local structure and the possible formation of $V_O$ defects, *in situ* time-resolved Ti $K$-edge XAS measurements were performed at elevated temperatures under 10% $H_2$/Ar flow, by employing the energy dispersive monochromator and N-type metal-oxide-semiconductor (NMOS) linear image sensor at BL-2.2 of the Siam photon source, SLRI, Thailand. Before collecting the XAS spectra, the sample ($K_2Ti_6O_{13}$ mixed with BN) was prepared as a pellet of 4 mm in diameter with the thickness less than 1 mm and put in the center of the heating cell. Initial spectra collected at several positions around the center of the pellet did not differ significantly from that at the center. These positions extended beyond the typical beam size of ~1.6 $mm^2$ (1 mm horizontally and 2 mm vertically).[44] So, it was assumed that the effect of microstructure inhomogeneity (e.g., holes, cracks, or thickness gradient) on the results should be minimal. The sample was heated up to 500 °C in air with the heating rate of 10 °C/min and held at 500 °C for 2 h to remove physically-sorbed water molecules from the surfaces. After that, the sample was slowly cooled down to 50 °C in air. The XAS spectrum, collected on the sample at this stage, represents the local structure prior to the reduction. Next, 10% $H_2$/Ar was fed into the chamber at 30 mL/min while the sample was simultaneously heated from 50 °C to 650 °C. The spectra were collected at every 50 °C interval. For simplicity, we report here only the spectra collected at 400, 500, 550, 600, and 650 °C which well represent the nature of the oxygen deficient $K_2Ti_6O_{13-x}$. Note that, the $K_2Ti_6O_{13-x}$ pellet at the end of the experiment turned into blue not only at the external surfaces but also at the interior. We did not observe cracks or holes visually either before or after the measurements. The blue color persisted for several months even in contact with atmospheric air.

To approximate the number of $V_O$ defects created in the sample during *in situ* EXAFS measurements at various temperatures, we calculated the radial distribution function (RDF) as implemented in EDARDF codes[45] to model the first coordination shell of Ti in $K_2Ti_6O_{13}$,

$$\chi(k) = S_0^2 \int_{R_{min}}^{R_{max}} \frac{G(R)}{kR^2} F(\pi, k, R) \sin[2kR + \phi(\rho, k, R)] dR, \quad (3)$$

where $S_0^2$ is the scaling factor taking account of amplitude reduction factor, $G(R)$ is the radial distribution function corresponding to the number of oxygen atoms located in the 1st shell around the absorber Ti atom, $F(\pi, k, R)$ is the backscattering amplitude of photoelectron due to the neighboring atom at the distance $R$, and $\phi(\pi, k, R)$ is the phase shift occurring from the absorber and the scattering atoms. The Gaussian 10% window function was used to set the range of

TABLE II. The Ti–O bond lengths in $TiO_6$ octahedra of $A_2Ti_6O_{13}$ ($A$ = Li, Na, K).[a]

| $Li_2Ti_6O_{13}$ | | | $Na_2Ti_6O_{13}$ | | | $K_2Ti_6O_{13}$ | | |
|---|---|---|---|---|---|---|---|---|
| $Ti^1$–O | $Ti^2$–O | $Ti^3$–O | $Ti^1$–O | $Ti^2$–O | $Ti^3$–O | $Ti^1$–O | $Ti^2$–O | $Ti^3$–O |
| 1.787 | 1.821 | 1.855 | 1.772 | 1.820 | 1.837 | 1.775 | 1.819 | 1.874 |
| (1.764) | (1.798) | (1.834) | (1.717) | (1.803) | (1.799) | (1.762) | (1.818) | (1.851) |
| 1.954 | 1.832 | 1.953 | 1.937 | 1.851 | 1.938 | 1.947 | 1.832 | 1.959 |
| (1.943) | (1.801) | (1.929) | (1.870) | (1.839) | (1.924) | (1.941) | (1.826) | (1.947) |
| 1.961 | 1.980 | 1.953 | 1.956 | 1.965 | 1.938 | 1.975 | 1.982 | 1.959 |
| (1.943) | (1.958) | (1.929) | (1.954) | (1.937) | (1.924) | (1.977) | (1.981) | (1.954) |
| 1.961 | 1.980 | 1.980 | 1.956 | 1.965 | 1.948 | 1.975 | 1.982 | 1.972 |
| (1.955) | (1.958) | (1.964) | (1.954) | (1.937) | (1.971) | (1.977) | (1.981) | (1.954) |
| 2.042 | 2.170 | 1.998 | 2.074 | 2.195 | 2.041 | 2.080 | 2.138 | 1.988 |
| (2.019) | (2.159) | (1.984) | (2.089) | (2.193) | (2.018) | (2.070) | (2.111) | (1.970) |
| 2.254 | 2.256 | 2.173 | 2.289 | 2.241 | 2.196 | 2.302 | 2.283 | 2.180 |
| (2.211) | (2.209) | (2.124) | (2.290) | (2.235) | (2.119) | (2.254) | (2.247) | (2.108) |

[a]Obtained by DFT calculations and the corresponding experimental values (Refs. 24, 26, and 29) (shown in parentheses). All values shown are in angstrom.

the first coordination shell with $R_{min} = 0.5$ Å and $R_{max} = 2.1$ Å. In this work, the theoretical phase shifts and scattering amplitudes for the first coordination shell were calculated using FEFF8.2 codes.[46,47] Here we used the radial distribution function method instead of fitting the EXAFS spectrum with conventional EXAFS equation (summation over many paths) because the range of 1st shell Ti–O bonds in $K_2Ti_6O_{13}$ is quite large (varying from 1.7 to 2.2 Å as shown in Table II) making modeling difficult. Thus, the coordination number $N$ located in the region between $R_{min}$ and $R_{max}$ is given by

$$N = \int_{R_{min}}^{R_{max}} G(R)dR. \tag{4}$$

### C. Calculation methods

We carried out first-principles calculations based on density functional theory (DFT) within the generalized gradient approximations parameterized by Perdew-Burke-Ernzerhof (GGA-PBE) for the exchange-correlation energy.[48] The electron-ion interactions were treated by the projector-augmented wave (PAW) method[49] as implemented in the VASP codes.[50,51] The cutoff energy for expanding the plane-wave basis set was set at 500 eV. All atoms in the cell were fully allowed to relax until the Hellmann-Feynman forces[52] became less than 0.01 eV/Å. In this work, the monoclinic $Na_2Ti_6O_{13}$ and $K_2Ti_6O_{13}$ 42-atoms unit cells with a space group of $C2/m$ were used for bulk calculations. For $Li_2Ti_6O_{13}$, the crystal structure is slightly modified (with respect to those of $Na_2Ti_6O_{13}$ and $K_2Ti_6O_{13}$) by shifting the Li atoms from Na/K positions by (0.0 0.5 0.0) in the fractional coordinate system.[24] The crystal structures of $K_2Ti_6O_{13}$ and $Li_2Ti_6O_{13}$ are depicted in Fig. 1. Note that the crystal structure of $Na_2Ti_6O_{13}$ (not shown) is similar to that of $K_2Ti_6O_{13}$. For bulk calculations, the Monkhorst-Pack scheme[53] with a sampling mesh of $3 \times 7 \times 3$ was used for $k$-space integrations. The calculated lattice parameters of $A_2Ti_6O_{13}$ ($A$ = Li, Na, K) are summarized in Table I, showing reasonable agreement with our own XRD results and with experimental values in the literature.

To compare our calculated structures with the measured Ti $K$-edge XANES spectra, the electronic transitions associated with the dipole selection rule were determined for each structure.[4,33,35] An X-ray absorbance $\mu(\omega)$ is given by the Fermi's golden rule

$$\mu \propto \sum_f \left|\langle f|D|i\rangle\right|^2 \delta(E_i - E_f + \omega), \tag{5}$$

where $|i\rangle$, $\langle f|$, $E_i$, and $E_f$ are the initial and final states and their corresponding energies, respectively. $\omega$ and $D$ are the photon frequency and dipole operator, respectively. For Ti $K$-edge, the initial state of the photoelectron is the core Ti 1$s$ state, i.e., $|i\rangle = |1s\rangle$, so the dipole-allowed final states have the symmetry of atomic $p$ states ($l = 1$). Because the initial state is localized at the absorbing Ti atom, only the final state wave function in the vicinity of the Ti is relevant. As described in Ref. 37, here we use just the calculated angular-momentum and site projected partial density of the final states with some broadening.

For XAS simulations, we employed FEFF8.2 codes[46,47] to generate the XANES and EXAFS spectrum associated with each crystal structure obtained from the first-principles (VASP codes) calculations. The FEFF8.2 codes are based on the multiple-scattering expansion with the muffin-tin potentials. The Hedin-Lundqvist approach[54] was used for the exchange-correlation function with an imaginary part of 0.5 eV to simulate the experimental broadening. The self-consistent calculations were performed in the sphere with radius of 7.0 Å around the absorber Ti atom.

## III. RESULTS AND DISCUSSION

### A. As-grown $A_2Ti_6O_{13}$ samples

All $A_2Ti_6O_{13}$ ($A$ = Li, Na, K) samples have the monoclinic unit cell with a space group of $C2/m$. The calculated lattice parameters are in good agreement with XRD results[22,29] as shown in Table I and in Fig S1 (see supplementary material). Note, however, that our samples were polycrystalline with relatively high surface area and small

crystallite sizes, while the literature values were typically from the single crystals. Since this difference precluded us from extracting the experimental bond lengths/bond angles, the calculated values were compared to the reported[22,29] (experimental) diffraction results instead. The crystal structures of $K_2Ti_6O_{13}$ and $Li_2Ti_6O_{13}$ are illustrated in Fig. 1, in which all Ti atoms are surrounded by six oxygen atoms forming distorted $TiO_6$ octahedra. While $K_2Ti_6O_{13}$ and $Na_2Ti_6O_{13}$ have the same crystal structures, Li atoms in $Li_2Ti_6O_{13}$ are shifted from the positions of Na/K as explained in Sec II C. The calculated Ti–O bond lengths in $A_2Ti_6O_{13}$ are in the ranges of 1.7–2.3 Å, in agreement with the experimental results as shown in Table II. Because the XRD technique requires long-range orderings to get the diffraction patterns, the formations of a small cluster of undesired phases as well as $V_O$ defects are generally overshadowed by the main signals from the crystalline part. In order to gain more information, we employed synchrotron XAS techniques covering both XANES and EXAFS regions, to investigate the oxidation state and the local environments of the selected absorber atom. Here, Ti *K*-edge XANES and EXAFS spectra were collected because Ti is a common element in all samples. Note that, there are three inequivalent Ti atoms in alkali hexatitanate structure with slight differences in the Ti–O bond lengths (see Table II). However, it is well known[22,29] that all three types of Ti atoms are surrounded by six oxygen atoms. The measured XAS spectra reflect the average environment of all Ti atoms in the samples as well as Ti on the surfaces.

We measured Ti *K*-edge XANES spectra of Ti foil, TiO, $Ti_2O_3$, and anatase-$TiO_2$ to use their absorption edges as references for $Ti^0$, $Ti^{2+}$, $Ti^{3+}$, and $Ti^{4+}$, respectively. The measured XANES spectra of as-grown samples are shown in comparison with those from standards in Fig. 2. It is clear that the absorption edges of all as-grown $A_2Ti_6O_{13}$ samples are close to that of anatase-$TiO_2$ (we added a vertical dashed line as a guide to the eye in Fig. 2). This confirms that the majority of Ti in all as-grown samples is $Ti^{4+}$. This further implies that Ti atoms in all samples should be six-fold coordinated with O atoms. In addition, the main features in the XANES spectra of all samples are quite similar. This indicates that the local structures of Ti atoms in all as-grown samples should be similar, in good agreement with reported X-ray diffraction results.[21,22,24,29,30] In finer detail, the difference among the measured XANES spectra is the intensities of the first two peaks (indicated by two arrows in the inset of Fig. 2). This slight variation can be attributed to the different cation species *A* as will be explained later.

Figure 3 shows the measured Ti *K*-edge EXAFS spectra in both *k*-space and R-space of as-grown $A_2Ti_6O_{13}$ samples. The EXAFS spectra were multiplied by $k^2$ to enhance the signal in the high *k* region. Fourier transformations (FT) as implemented in DEMETER package[43] were applied with the Hanning window between $2.5 < k < 6.0$ Å$^{-1}$ to obtain the R-space representation of the EXAFS spectra. The similarity of EXAFS spectra in both *k*-space and R-space of the as-grown $A_2Ti_6O_{13}$ ($A$ = Na, K) implies that the local structures of Ti atoms in all as-grown samples are similar. Slight differences, however, were observed in the R-space EXAFS spectrum of $Li_2Ti_6O_{13}$ with a reduction in the intensity of the first peak compared to others.

The intensities of EXAFS spectra in R-space are related to the type and number of scattering atoms for each scattering shell. Because the first-shell of Ti atoms is only composed of O atoms, this finding provides the direct evidence that there are lower numbers of first-shell scattering O atoms in the bulk. These missing O atoms (i.e., $V_O$ defects) were not detected in neutron diffraction studies[22,24] of $Li_2Ti_6O_{13}$ similarly prepared, likely due to the limited concentration. We propose that the preparation in $LiNO_3$ flux might generate a rather reducing environment, such that a small portion of O atoms is unintentionally removed from the lattice sites of $Li_2Ti_6O_{13}$. The formation of $V_O$ defects due to heat-treatment under the reducing (alkali-vapor) atmosphere has also been

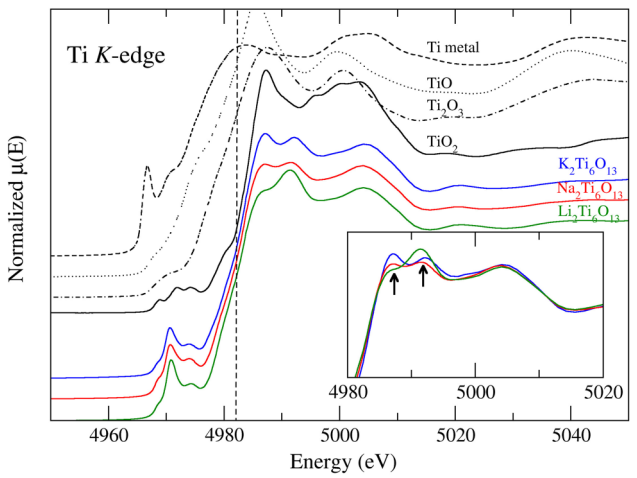


FIG. 2. The measured Ti *K*-edge XANES spectra of as-grown $K_2Ti_6O_{13}$ (blue), $Na_2Ti_6O_{13}$ (red), $Li_2Ti_6O_{13}$ (green) samples and standards, including anatase-$TiO_2$, $Ti_2O_3$, TiO, and Ti foil. The vertical dashed line indicates the absorption edge of as-grown $A_2Ti_6O_{13}$ ($A$ = Li, Na, K) samples. The inset shows the zoom-in of the peaks near the absorption edge.

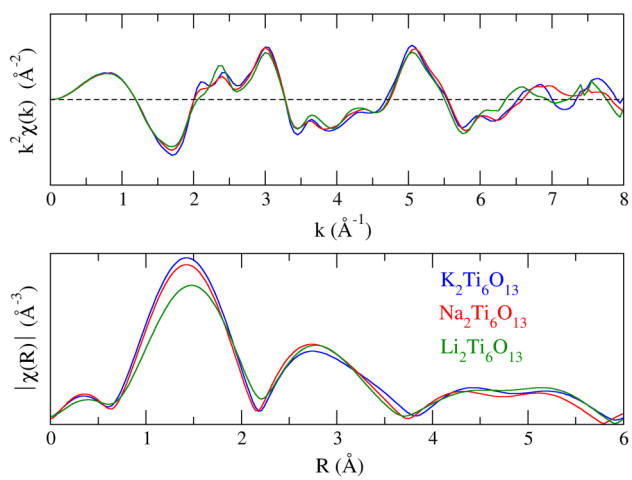


FIG. 3. The measured Ti *K*-edge EXAFS spectra in *k*-space (top) and R-space (bottom) of as-grown $K_2Ti_6O_{13}$ (blue), $Na_2Ti_6O_{13}$ (red), and $Li_2Ti_6O_{13}$ (green) samples. The Hanning window in the range of 2.5 to 6.0 Å$^{-1}$ was used for Fourier transform.

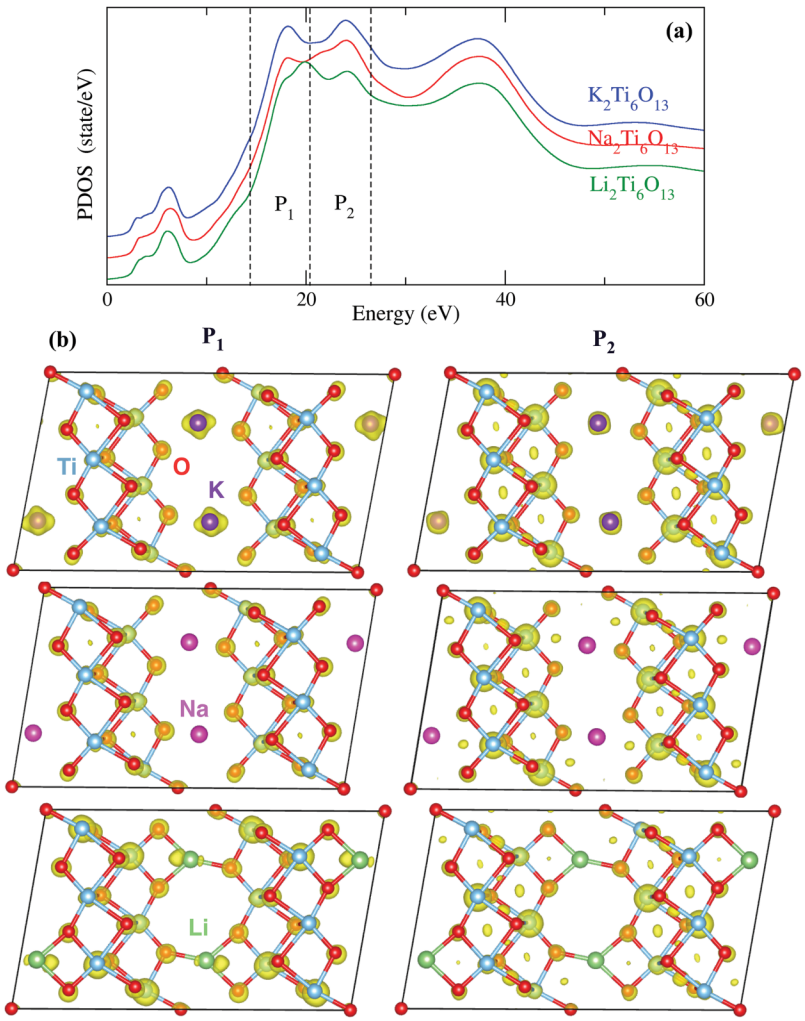


FIG. 4. (a) The calculated angular momentum *p* projected PDOS of Ti atoms in $K_2Ti_6O_{13}$, $Na_2Ti_6O_{13}$, and $Li_2Ti_6O_{13}$. (b) The electron densities associated with two energy regions indicated by $P_1$ and $P_2$ for $K_2Ti_6O_{13}$, $Na_2Ti_6O_{13}$, and $Li_2Ti_6O_{13}$ are presented in the left and right columns, respectively.

suggested[55] in $K_{0.8}M_{0.4}Ti_{1.6}O_4$ (M = Ni, Cu, and Zn) with the related lepidocrocite structure. By the same analogy, one can deduce that as-grown $Li_2Ti_6O_{13}$ is comparatively richer in $V_O$ defects than $Na_2Ti_6O_{13}$ and $K_2Ti_6O_{13}$.

To relate the measured XANES spectra to the electronic structures of $A_2Ti_6O_{13}$, we calculated the angular momentum projected density of states (PDOS) to simulate the XANES spectrum, as described in Sec. II, associated with each crystal structure. Figure 4(a) shows the calculated spectra of $A_2Ti_6O_{13}$. The calculated XANES spectra of $Na_2Ti_6O_{13}$ and $K_2Ti_6O_{13}$ that have almost the same crystal structures show only a slight difference in the near-edge regions, the regions labeled P1 and P2. On the other hand, the spectrum in that region of $Li_2Ti_6O_{13}$ (whose $Li^+$ ions positions are significantly different from those of $Na^+/K^+$ ions) is remarkably different from those of $Na_2Ti_6O_{13}$ and $K_2Ti_6O_{13}$. Because the local environments of Ti atoms in $A_2Ti_6O_{13}$ are similar (see Table II), the differences in the near-edge regions of XANES spectra must be mainly a result of the type of cation species in the tunnel. We can see that the calculated XANES spectra nicely reproduced the main features of the measured XANES spectra.

In Fig. 4(b), the charge densities associated with the two energy regions [P1 and P2 in Fig. 4(a)] are shown. The charge densities of $K_2Ti_6O_{13}$ and $Na_2Ti_6O_{13}$ corresponding to P1 and P2 energy regions are quite similar, except those localized around the $Na^+/K^+$ ions. (Note, however, that only the charge localized on the absorber atom, i.e., Ti, contributes to the XANES spectrum.) In contrast, the charge density of the hexatitanate framework in $Li_2Ti_6O_{13}$ corresponding to P1 and P2 regions is quite different from the other two compounds. These charge density plots illustrate that the different cations, i.e., $K^+/Na^+$ vs $Li^+$ significantly affect the electron distribution in the crystal, which results in the different features of XANES spectra in P1 and P2 regions. Such difference could be the electronic origin responsible for the *A*-dependent performance in some applications of $A_2Ti_6O_{13}$ such as the lithium-ion battery.[22,56]

### B. Reduced $K_2Ti_6O_{13-x}$ samples under exposure to $H_2$ gas

Since the catalytic ketonization of acetic acid over $K_2Ti_6O_{13}$ (and other reducible oxides)[57] is dependent on the formation and amount of $V_O$ defects at elevated temperatures (to be published), we exemplify here the intuitive use of XAS to study the formation and quantification of $V_O$ defects in $K_2Ti_6O_{13-x}$. In this work, we performed *in situ* time-resolved Ti *K*-edge XAS measurements to investigate the oxidation states and local structures of $K_2Ti_6O_{13-x}$ samples reduced at several temperatures, i.e., 50, 400, 500, 550, 600,

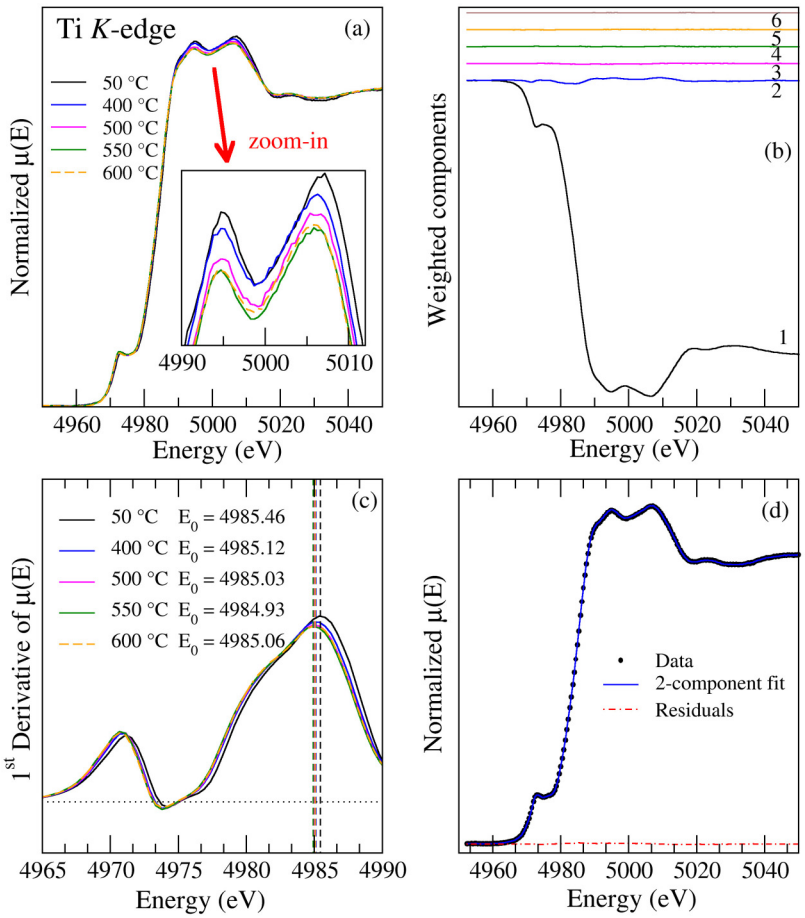


FIG. 5. (a) The measured *in situ* Ti *K*-edge XANES spectra of $K_2Ti_6O_{13}$ sample reduced under the flowing of 10% $H_2$/Ar at different reduction temperatures. The inset shows the zoom-in of the peaks near the absorption edge. (b) The first six components from PCA calculation weighted by their eigenvalues. (c) The associated 1st derivative of *in situ* Ti *K*-edge XANES spectra at different reduction temperatures. (d) A representative spectrum (dotted line) superimposed with the linear combination of first two components (filled blue line) where the residual are shown in the dashed-dotted red line.

and 650 °C, under 10%$H_2$/Ar. Figure 5(a) shows the measured *in situ* time-resolved Ti *K*-edge XANES spectra. The absorption edges of XANES spectra of all samples take place almost at the same position, indicating that the majority of Ti atoms in all $K_2Ti_6O_{13-x}$ samples remains $Ti^{4+}$. The slight shift of the edge to lower energy at different temperatures [see Fig. 5(c)] corresponds to the existence of a small fraction of $Ti^{3+}$. Our result is consistent with the widely accepted model[5,6,8–10] that only the minority of Ti atoms on the surface gets reduced to $Ti^{3+}$, leaving the majority of Ti atoms to remain unchanged in $Ti^{4+}$ state. A detailed comparison of the spectra among different samples shows that the intensities of the first two peaks are decreased and the absorption edges shift to lower energy as the reduction temperature increases from 50 to 550 °C [inset of Fig. 5(a)] prior to the slight increase at higher temperatures. This indicates that the maximum amount of $Ti^{3+}$ is observed at a reduction temperature of 550 °C. Note that, the XANES spectrum at 650 °C (not shown) is similar to that at 600 °C. The first two peaks represent the signature of the Ti atoms in the ideal configuration of $K_2Ti_6O_{13}$. Therefore, the Ti atoms neighboring to $V_O$ defects would have distinct XANES features and result in the reduction of these two peaks.

Furthermore, principal component analysis (PCA) as implemented in ATHENA package[43] was used to analyze the distinct phase during the reduction at high temperatures. The six eigenvectors sorted in the descending order of their respective eigenvalues from PCA calculation are illustrated in Fig. 5(b). It can be seen that the first component clearly dominates the spectra with a small contribution from the second component as depicted in Fig. 5(d). This is in good agreement with the observed small shift of the absorption edge to lower energy. Therefore, a small amount of $Ti^{3+}$ presented in the sample could be expected. In addition, the calculated Ti *K*-edge XANES spectra of $K_2Ti_6O_{13}$ with and without the $V_O$ defect are shown in Fig. 6. Note that the $V_O$ defect was created in a 42-atom $K_2Ti_6O_{13}$ unit cell, which was used to simulate the XANES spectra by using FEFF8.2 codes. It can be seen that both spectra are analogous; however, a small difference in the low energy regions is observed reflecting that the present of $V_O$ in $K_2Ti_6O_{13}$ does not significantly affect the shape of XANES spectra in agreement with the observed spectra. Next, we used the *in situ* time-resolved Ti *K*-edge

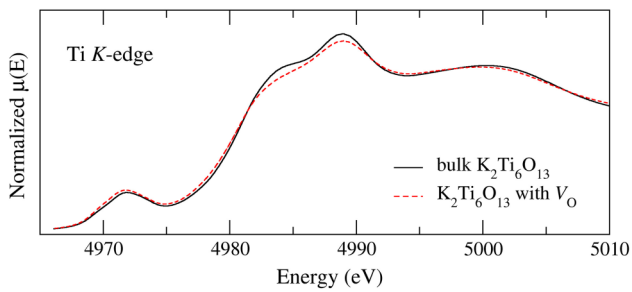


FIG. 6. The calculated Ti *K*-edge XANES spectra of $K_2Ti_6O_{13}$ with and without the $V_O$ defect.

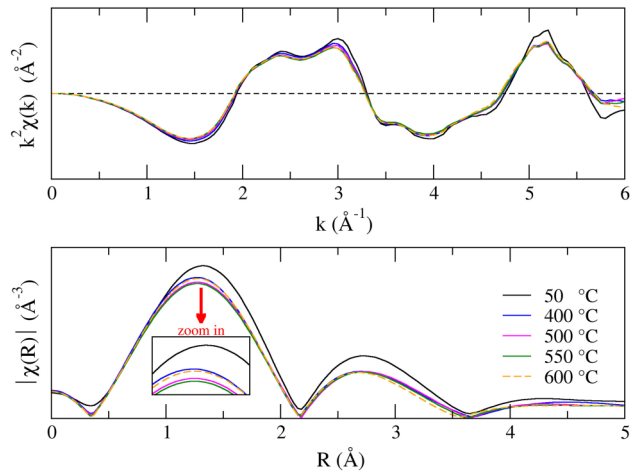


FIG. 7. The measured *in situ* Ti *K*-edge EXAFS spectra in *k*-space (top) and R-space (bottom) of $K_2Ti_6O_{13-x}$ sample under exposure to 10% $H_2$/Ar at different temperatures. The inset shows the amplification of the first peak. The Hanning window in the range of 2.5 to 6.0 $Å^{-1}$ was used for Fourier transform.

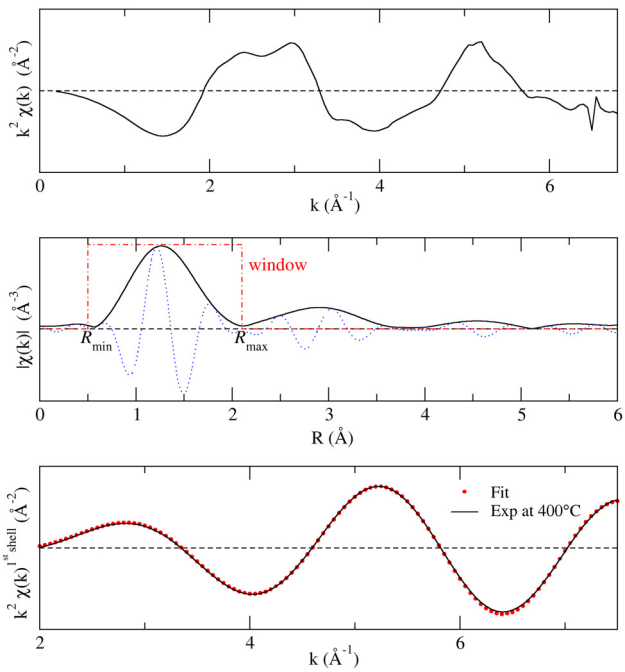


FIG. 8. The measured Ti *K*-edge EXAFS spectrum at 50 °C in k space (top) and R space (middle). The Gaussian 10% window function in the range of 0.5 to 2.1 $Å^{-1}$ is used for back-Fourier transform to set the range of first coordination shell. The bottom panel represents the 1st shell EXAFS spectrum obtained from back-Fourier transform (black filled line) accompanying with the fitting from Eq. (3) (red dotted line).

EXAFS spectra to approximate the number of $V_O$ defects introduced during reduction at high temperatures.

Figure 7 illustrates the *in situ* time-resolved Ti *K*-edge EXAFS spectra in *k*-space (top) and R-space (bottom) of $K_2Ti_6O_{13-x}$. For the EXAFS spectra in the R-space, the intensities of the first two peaks are decreased as the reduction temperatures increase from 50 °C to 550 °C. This is similar to what we have observed in the *in situ* XANES spectra. As mentioned earlier, the intensities of EXAFS spectra in the R-space are directly related to the type and number of scattering atoms in each scattering path. By considering the local geometry around Ti atoms in $K_2Ti_6O_{13-x}$, we can assign the first peak at ~1.4 Å to the single scattering path involving the first-neighboring six O atoms (Ti–O–Ti). Next, the second peak at ~2.7 Å is assigned to the single scattering from absorber Ti atom to another Ti atom (Ti–Ti′–Ti). Note that the peak positions in R-space are not really the bond distances between the scattering atoms, because the scattering process does not take place at the center of each atom. Since O atoms will be removed at elevated reduction temperatures, weaker intensities of the first peak of EXAFS spectra in R-space are expected as depicted in Fig. 7. Therefore, our XAS results provide an evidence for the formation of $V_O$ defects in $K_2Ti_6O_{13-x}$ upon the reduction by $H_2$ at elevated temperatures.

The *in situ* time-resolved XAS spectra has allowed us to semi-quantitatively determine the number of $V_O$ defects at the temperature where they are generated, otherwise difficult to obtain by other methods. As displayed in Eq. (3), the RDF function of the first coordination shell of Ti in $K_2Ti_6O_{13}$ can be extracted by (1) using Fourier and back-Fourier transform to extract the 1st shell EXAFS spectra from the measured EXAFS spectra at different temperatures and (2) fitting the 1st shell EXAFS spectra with Eq. (3) by the least-squares method as implemented in EDARDF codes.[45] In the fitting, we used the crystal structure obtained from VASP codes to generate the FEFF input, which is further used to calculate the phase shifts and scattering amplitudes for the first scattering shell (Ti–O). Figure 8 illustrates all processes mentioned above for the measured EXAFS spectrum at 50 °C as an example. The RDF of 1st shell EXAFS spectra reduced at different temperatures obtained from the fitting with Eq. (3) is depicted in Fig. 9. As shown in Eq. (4), the coordination number of the 1st shell is related to the area under the graph. In this case, we would like to determine the number of $V_O$ defects created in the sample at different reduction temperatures with respect to the sample before reduction (i.e., 50 °C). We then calculated the area under the graph at different temperatures with respect to that at 50 °C. The calculated relative areas are 0.791, 0.775, 0.766, and 0.805 for 400 °C:50 °C, 500 °C:50 °C, 550 °C:50 °C, and 600 °C:50 °C, respectively. It is clearly seen that the coordination number reaches the lowest value at the reduction temperature of ~550 °C. This is consistent with the highest shift of the absorption edge to the lower energy as mention previously, which indicates the highest amount of $Ti^{3+}$ presented in the sample.

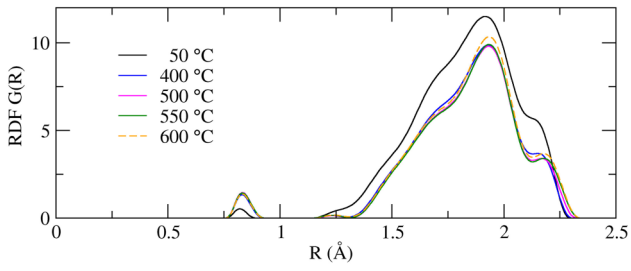


FIG. 9. The radial distribution function (RDF) of the samples reduced at different temperatures obtained from the fitting with Eq. (3).

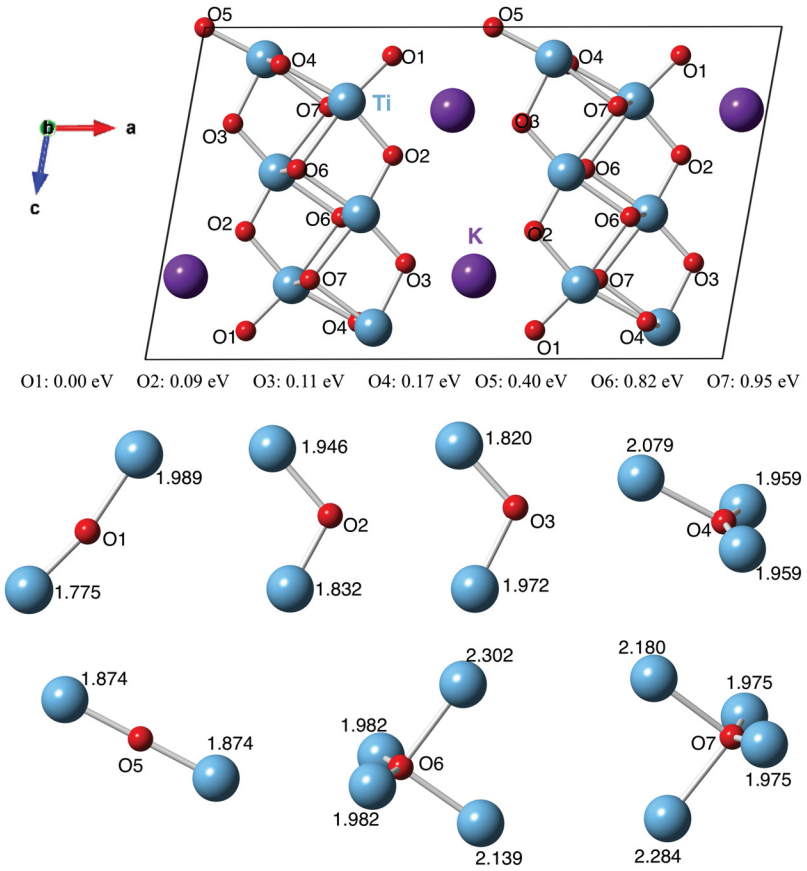


FIG. 10. (Top) Illustration of the crystallographically inequivalent O site associated with the energy used to create $V_O$ defects. The labels O1 to O7 are in the order of the lowest energy to the highest energy. The values shown are the relative energies used to create $V_O$ defect at different sites with respect to the lowest energy site, i.e., O1. (Bottom) The local structures of seven inequivalent O sites. The bond length between O and its first-neighboring Ti atoms are shown in angstrom.

Based on $K_2Ti_6O_{13}$ crystal structure, there are seven local geometry types of O atoms with the Ti nearest neighbor ranging from 2 to 4 atoms as seen in Fig. 10. Basically, we can estimate the number of missing O atoms, i.e., $V_O$ defects, based on the area under the graph in Fig. 9. To estimate the number of $V_O$ defects created in the samples at elevated temperatures with respect to that at 50 °C, the relative area must be subtracted from 1 and divided by ~2.714 (19 Ti–O bonds per seven types of O), which represents the number of decreasing Ti–O bonds after the removal of one oxygen atom. We found that 8.51, 9.05, 9.26, and 7.68 at. % of O atoms are removed from the samples treated by $H_2$ at 400 °C, 500 °C, 550 °C, and 600 °C, respectively. If we assume that all of $V_O$ defects are active and each $V_O$ reduces two Ti atoms, this set the upper limit of reduced Ti (i.e., $Ti^{3+}$) to 23.1, 24.6, 25.1, and 20.8 at. % for 400 °C, 500 °C, 550 °C, and 600 °C-treated samples, respectively. We have to note that these calculated values might be too high because we assume that the amplitude reduction factors are constant for all temperatures. Due to limitation of beam time, we propose that this could be corrected by measuring the EXAFS spectra with and without flowing of $H_2$ gas to determine the amplitude reduction factors of EXAFS spectra at different temperatures. Nevertheless, the analysis of $V_O$ by XAS is somewhat more straightforward compared to other commonly employed techniques such as temperature-programmed desorption (TPD) (detecting the $O_2$ gas evolved) or EPR (detecting e.g., $O_2^-$ radicals from sorbed gas). The information obtained is from the bulk, in contrast to XPS (i.e., via $Ti^{3+}$ signal) analyzing surfaces. Additionally, XAS is capable of providing a detailed atomic structure including Ti–O bond lengths in amorphous materials with limited long-range ordering, in contrast to, e.g., typical neutron diffraction experiments. In principle, our analysis with XAS could be applicable to other materials (including $TiO_2$) as well.

It is important to emphasize that our approach is semi-quantitative, since the amount of $V_O$ defects at elevated temperatures is relative to the one at 50 °C. Upon increasing the reduction temperatures from 50 °C to 550 °C, the amount of $V_O$ defects increases, but followed by a decrease at the reduction temperatures above 550 °C. This indicates that the maximum amount of $Ti^{3+}$ is at 550 °C which agrees well with the shift of the absorption edge of *in situ* XANES spectra. The reduction of $V_O$ defects at temperatures above 550 °C could be attributed to the diffusion of oxygen released from the surface of the heating cell into the sample. Furthermore, our result suggests that heating the sample under $H_2$ at 550 °C gives the highest catalytic activity, which can help us to optimize the reduction temperature. Even with this upper bound calculation, the majority oxidation state of Ti in all samples is clearly still 4+. However, the blue color of the reduced sample at the end of the experiment is a strong and widely accepted indication that $Ti^{3+}$ is present in materials.[58,59]

To gain a deeper understanding of the formation of $V_O$ defect in $K_2Ti_6O_{13}$, first-principles DFT calculations were conducted. A supercell approach with the supercell size of 126 atoms was used to reduce the defect-defect interactions arising from the neighboring cell. We found that $V_O$ defect is a double shallow donor, meaning that it can donate two

electrons to the conduction band. Hereafter, the calculations involving $V_O$ defect were carried out in 2+ charge state. Due to a low symmetry of $K_2Ti_6O_{13}$, there are seven inequivalent O sites labeled as O1–O7 in Fig. 10. The labels are ordered according to the energy used to remove each O atom from its lattice site, i.e., the lowest energy for O1 and the highest energy for O7 (see supplementary material). The relative energies used to create the $V_O$ defect at different sites with respect to the lowest one are shown in Fig. 10. The oxygen atoms near the tunnel, especially O1–O3, can be easily removed compared to other oxygen atoms. This is because O1–O3 bond with only two Ti atoms. On the other hand, O6 and O7 each bond with four Ti atoms, making them more stable and requiring high energy to be removed. Our finding in $K_2Ti_6O_{13}$, where the most active O atom locates nearest to the tunnel and possessing the smallest coordination number, is similar to that reported previously for $Na_2Ti_3O_7$ with related structure.[40,60] Interestingly, O5, which is two-fold coordinated, is more stable than O4, which is three-fold coordinated. On a closer look we can see that, unlike O1–O3, O5 is linearly bound with two Ti atoms similar to the case of a $CO_2$ molecule. To remove O5, it requires somewhat higher energy to break the symmetry between Ti and O.

In order to compare our calculations with the experimental EXAFS spectra, we removed one oxygen atom at the O1 site (the lowest energy configuration) to create $V_O$ defect in 42-atom $K_2Ti_6O_{13}$ unit cell and allowed the structure to relax. Note that we used the 42-atom unit cell instead of the 126-atom supercell because the number of $V_O$ defects created in the 42-atom unit cell is ~2.38 at. %, which is close to what we have observed in the experiment. Then, the optimized structures with/without the $V_O$ defect were used as the input coordinates for FEFF codes to simulate the EXAFS spectra. Figure 11 illustrates the simulated Ti *K*-edge EXAFS spectra of $K_2Ti_6O_{13}$ (without defect) and $K_2Ti_6O_{13}$ with $V_O$ defect in *k*-space and R-space. We can see that the removal of an oxygen atom from its lattice site, i.e., the generation of $V_O$ defect, affects the intensities of the first two peaks of EXAFS spectra in R-space as expected. In addition, we performed the Bader charge analysis calculations[61–63] to investigate the charge on Ti atoms in the supercell before and after creating $V_O$ defect. We found that the averaged charge on Ti atoms in the supercell containing $V_O$ defect is quite similar to that in supercell without defect (not shown), serving as another evidence that the oxidation state of Ti atoms in the supercell with and without $V_O$ defect remains unchanged, i.e., $Ti^{4+}$. This agrees well with the observed *in situ* XANES spectra as described above.

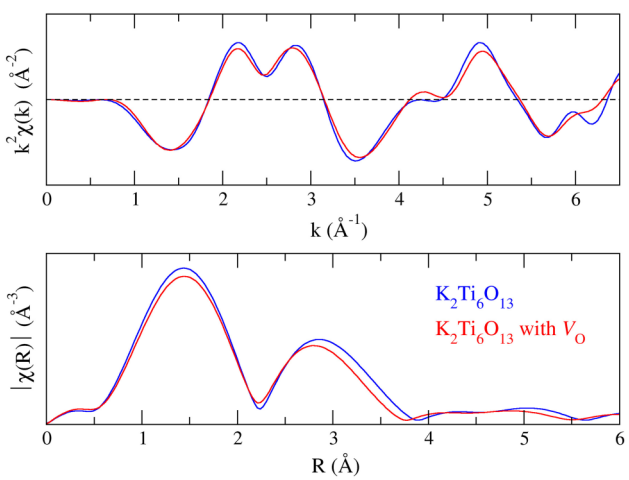


FIG. 11. The calculated EXAFS spectra in *k*-space (top) and R-space (bottom) of bulk $K_2Ti_6O_{13}$ (blue) and $K_2Ti_6O_{13}$ with one oxygen vacancy (red). The Hanning window in the range of 2.5 to 6.0 $Å^{-1}$ was used for Fourier transform.

## IV. CONCLUSION

Local structures of Ti atoms in alkali hexatitanate before and after exposure to $H_2$ gas were investigated by using XAS measurements (including both XANES and EXAFS regions) in conjunction with first principles density functional calculations. For as-grown $A_2Ti_6O_{13}$ ($A$ = Li, Na, K), we found that all samples give similar features of XANES spectra indicating that the local structures of Ti are analogous. By comparing the absorption edge with the standards, we found that the majority of Ti in all as-grown samples is $Ti^{4+}$. The slight differences in measured XANES spectra are assigned to the different cation species, i.e., $Li^+$ vs $Na^+/K^+$. We demonstrated the use of XAS measurements to compare the relative proportion of $V_O$ defects already existing in the as-grown samples. The reduction and the formation of $V_O$ defects in $K_2Ti_6O_{13-x}$ were studied in more details by *in situ* time-resolved XAS measurements where the samples were exposed to $H_2$ at 50-650 °C. Based on *in situ* XANES measurements, the majority of Ti atoms in the sample after exposure to $H_2$ gas remain as $Ti^{4+}$. In addition, we presented direct evidence regarding the formation of $V_O$ defects in $K_2Ti_6O_{13-x}$ by means of *in situ* EXAFS measurements. The semi-quantitative determination of the number of $V_O$ defects shows that the highest value is reached at the reduction temperature of ~550 °C presumably associated with the highest reactivity of the sample. Based on DFT calculations, the removal of the oxygen atom near the tunnel is energetically most favorable. The EXAFS spectrum simulated from the structure with the $V_O$ defect is in agreement with the experimental results. The application of *in situ* EXAFS measurements reported here is an intuitive way to estimate the proportion of reduced Ti atoms at elevated temperatures, otherwise difficult to obtain (or obtainable indirectly at most). Our results enable a comparison with other *ex situ* characterizations typically conducted in a laboratory including temperature-programmed reduction by $H_2$ ($H_2$ TPR), optical measurements by diffused reflectance UV (DRUV), and allow the better understanding of a structure-property relationship (e.g., ketonization of acetic acid). Results will be reported elsewhere.

## SUPPLEMENTARY MATERIAL

See supplementary material for Fig. S1 and Table S1.

## ACKNOWLEDGMENTS

T.M. acknowledges the financial support from the National Research Council of Thailand, Grant 2558A11802038.

J.T., A.B., and P.R. acknowledge the financial support from Kasetsart University Research and Development Institute (KURDI). J.K. acknowledges the financial support from the Institute for Promotion of Science and Technology (DPST Research Grant 10/2557). J.T. would like to thank Dr. Chanapa Kongmark for fruitful discussion about PCA analysis.

[1]T. Maluangnont, P. Arsa, and T. Sooknoi, J. Solid State Chem. **256**, 219 (2017).
[2]T. Maluangnont, P. Arsa, K. Limsakul, S. Juntarachairot, S. Sangsan, K. Gotoh, and T. Sooknoi, J. Solid State Chem. **238**, 175 (2016).
[3]A. Boonchun, P. Reunchan, and N. Umezawa, Phys. Chem. Chem. Phys. **18**, 30040 (2016).
[4]J. T-Thienprasert, S. Klaithong, A. Niltharach, A. Worayingyong, S. Na-Phattalung, and S. Limpijumnong, Curr. Appl. Phys. **11**, S279 (2011).
[5]G. Liu, L. Z. Wang, C. H. Sun, X. X. Yan, X. W. Wang, Z. G. Chen, S. C. Smith, H. M. Cheng, and G. Q. Lu, Chem. Mater. **21**, 1266 (2009).
[6]G. Liu, L. Z. Wang, C. H. Sun, Z. G. Chen, X. X. Yan, L. Cheng, H. M. Cheng, and G. Q. Lu, Chem. Commun. 1383 (2009).
[7]T. Maluangnont, C. Dararat, T. Kulrat, S. Soontontaweesub, T. Anothaiwalaikul, P. Bunprechawong, R. Chanda, J. Kanchanawarin, P. Kidkhunthod, and T. Sooknoi, Catal. Commun. **102**, 123 (2017).
[8]L. N. Kong, Z. Q. Jiang, C. H. Wang, F. X. Wan, Y. Y. Li, L. Z. Wu, J. F. Zhi, X. T. Zhang, S. J. Chen, and Y. C. Liu, ACS Appl. Mater. Interfaces **7**, 7752 (2015).
[9]H. Liu, H. T. Ma, X. Z. Li, W. Z. Li, M. Wu, and X. H. Bao, Chemosphere **50**, 39 (2003).
[10]G. Lu, A. Linsebigler, and J. T. Yates, J. Phys. Chem. **98**, 11733 (1994).
[11]D. C. Sinclair, J. M. S. Skakle, F. D. Morrison, R. I. Smith, and T. P. Beales, J. Mater. Chem. **9**, 1327 (1999).
[12]S. Andersson and A. D. Wadsley, Acta Cryst. **15**, 201 (1962).
[13]S. Andersson and A. D. Wadsley, Acta Cryst. **15**, 194 (1962).
[14]A. D. Wadsley and S. Andersson, Nature **192**, 551 (1961).
[15]S. Andersson and A. D. Wadsley, Acta Cryst. **14**, 1245 (1961).
[16]S. Andersson and A. D. Wadsley, Acta Chem. Scand. **15**, 663 (1961).
[17]Q. Zhang, Y. P. Guo, K. Guo, T. Y. Zhai, and H. Q. Li, Chem. Commun. **52**, 6229 (2016).
[18]Z. Chen, Y. Wu, Y. Wei, and H. Mimura, J. Radioanal. Nucl. Chem. **307**, 931 (2016).
[19]Q. Wang, Q. J. Guo, and B. Li, RSC Adv. **5**, 66086 (2015).
[20]K. Shen and M. Wagemaker, Inorg. Chem. **53**, 8250 (2014).
[21]J. C. Perez-Flores, F. Garcia-Alvarado, M. Hoelzel, I. Sobrados, J. Sanz, and A. Kuhn, Dalton Trans. **41**, 14633 (2012).
[22]J. C. Perez-Flores, C. Baehtz, M. Hoelzel, A. Kuhn, and F. Garcia-Alvarado, Phys. Chem. Chem. Phys. **14**, 2892 (2012).
[23]J. C. Pérez-Flores, A. Kuhn, and F. García-Alvarado, J. Power Sources **196**, 1378 (2011).
[24]K. Kataoka, J. Awaka, N. Kijima, H. Hayakawa, K. Ohshima, and J. Akimoto, Chem. Mater. **23**, 2344 (2011).
[25]Q. Wang, Z. H. Guo, and J. S. Chung, Mater. Res. Bull. **44**, 1973 (2009).
[26]L. M. Torres-Martinez, I. Juarez-Ramirez, K. Del Angel-Sanchez, L. Garza-Tovar, A. Cruz-Lopez, and G. Del Angel, J. Sol-Gel Sci. Technol. **47**, 158 (2008).
[27]I. Becker, I. Hofmann, and F. A. Muller, J. Eur. Ceram. Soc. **27**, 4547 (2007).
[28]T. Shimizu, T. Morita, H. Yanagida, and K. Hashimoto, J. Ceram. Soc. Jpn. **85**, 189 (1977).
[29]H. Cid-Dresdner and J. M. Buerger, Z. Kristallogr. Cryst. Mater. **117**, 411 (1962).
[30]K. Kataoka, N. Kijima, and J. Akimoto, Inorg. Chem. **52**, 13861 (2013).
[31]F. Farges, G. E. Brown, and J. J. Rehr, Geochim. Cosmochim. Acta **60**, 3023 (1996).
[32]N. Schwertfager, N. Pandech, M. Suewattana, J. T-Thienprasert, and S. Limpijumnong, Ferroelectrics **490**, 159 (2016).
[33]J. T-Thienprasert, S. Rujirawat, W. Klysubun, J. N. Duenow, T. J. Coutts, S. B. Zhang, D. C. Look, and S. Limpijumnong, Phys. Rev. Lett. **110** (2013).
[34]A. Tongraar, J. T-Thienprasert, S. Rujirawat, and S. Limpijumnong, Phys. Chem. Chem. Phys. **12**, 10876 (2010).
[35]J. T-Thienprasert, S. Rujirawat, J. Nukeaw, and S. Limpijumnong, Comp. Mater. Sci. **49**, S37 (2010).
[36]J. T-Thienprasert, J. Nukeaw, A. Sungthong, S. Porntheeraphat, S. Singkarat, D. Onkaw, S. Rujirawat, and S. Limpijumnong, Appl. Phys. Lett. **93** (2008).
[37]S. Limpijumnong, S. Rujirawat, A. Boonchun, M. F. Smith, and B. Cherdhirunkorn, Appl. Phys. Lett. **90**, 103113 (2007).
[38]M. Catti, I. Pinus, and A. Scherillo, J. Solid State Chem. **205**, 64 (2013).
[39]Y. Wang, T. Sun, D. J. Yang, H. W. Liu, H. M. Zhang, X. D. Yao, and H. J. Zhao, Phys. Chem. Chem. Phys. **14**, 2333 (2012).
[40]Y. Wang, H. W. Liu, H. M. Zhang, X. D. Yao, and H. J. Zhao, Chem. Phys. Lett. **511**, 82 (2011).
[41]J. Li, Y. C. Zhang, and M. Zhang, Mater. Lett. **79**, 136 (2012).
[42]S. Papp, L. Korosi, V. Meynen, P. Cool, E. F. Vansant, and I. Dekany, J. Solid State Chem. **178**, 1614 (2005).
[43]B. Ravel and M. Newville, J. Synchrotron Radiat. **12**, 537 (2005).
[44]Y. Poo-arporn, P. Chirawatkul, W. Saengsui, S. Chotiwan, S. Kityakarn, S. Klinkhieo, J. Hormes, and P. Songsiriritthigul, J. Synchrotron Radiat. **19**, 937 (2012).
[45]A. Kuzmin, Phys. B Condens. Matter **208-209**, 175 (1995).
[46]A. L. Ankudinov, C. E. Bouldin, J. J. Rehr, J. Sims, and H. Hung, Phys. Rev. B **65**, 104107 (2002).
[47]A. L. Ankudinov, B. Ravel, J. J. Rehr, and S. D. Conradson, Phys. Rev. B **58**, 7565 (1998).
[48]J. P. Perdew, K. Burke, and M. Ernzerhof, Phys. Rev. Lett. **77**, 3865 (1996).
[49]G. Kresse and D. Joubert, Phys. Rev. B **59**, 1758 (1999).
[50]G. Kresse and J. Furthmüller, Comp. Mater. Sci. **6**, 15 (1996).
[51]G. Kresse and J. Furthmüller, Phys. Rev. B **54**, 11169 (1996).
[52]R. P. Feynman, Phys. Rev. **56**, 340 (1939).
[53]H. J. Monkhorst and J. D. Pack, Phys. Rev. B **13**, 5188 (1976).
[54]L. Hedin and S. Lundqvist, in *Solid State Physics*, edited by D. T. Frederick Seitz and E. Henry (Academic Press, 1970), Vol. 23, p. 1.
[55]T. Maluangnont, N. Chanlek, T. Suksawad, N. Tonket, P. Saikhamdee, U. Sukkha, and N. Vittayakorn, Dalton Trans. **46**, 14277 (2017).
[56]R. Dominko, L. Dupont, M. Gaberšček, J. Jamnik, and E. Baudrin, J. Power Sources **174**, 1172 (2007).
[57]T. N. Pham, T. Sooknoi, S. P. Crossley, and D. E. Resasco, ACS Catal. **3**, 2456 (2013).
[58]B. Bharti, S. Kumar, H.-N. Lee, and R. Kumar, Sci. Rep. **6**, 32355 (2016).
[59]M. S. Hamdy, R. Amrollahi, and G. Mul, ACS Catal. **2**, 2641 (2012).
[60]Y. An, Z. Li, H. Xiang, Y. Huang, and J. Shen, Cent. Eur. J. Phys. **9**, 1488 (2011).
[61]M. Yu and D. R. Trinkle, J. Chem. Phys. **134**, 064111 (2011).
[62]W. Tang, E. Sanville, and G. Henkelman, J. Phys. Condens. Matter **21**, 084204 (2009).
[63]G. Henkelman, A. Arnaldsson, and H. Jónsson, Comp. Mater. Sci. **36**, 354 (2006).